

Supervised segmentation of NO₂ plumes from individual ships using TROPOMI satellite data

Solomiia Kurchaba
 s.kurchaba@liacs.leidenuniv.nl
 Leiden University
 Leiden, The Netherlands

Jasper van Vliet
 Human Environment and Transport
 Inspectorate (ILT)
 Utrecht, The Netherlands

Fons J. Verbeek
 Leiden University
 Leiden, The Netherlands

Jacqueline J. Meulman
 Stanford University
 Stanford, CA, USA
 Leiden University
 Leiden, The Netherlands

Cor J. Veenman
 Leiden University
 Leiden, The Netherlands
 TNO
 The Hague, The Netherlands

ABSTRACT

Starting from 2021, the International Maritime Organization significantly tightened the NO_x emission requirements for ships entering the Baltic and North Sea waters. Since all methods currently used for the ships' compliance monitoring are costly and require proximity to the ship, the performance of a global and continuous monitoring of the emission standards' fulfillment has been impossible up to now. A promising approach is the use of remote sensing with the recently launched TROPOMI/S5P satellite. Due to its unprecedently high spatial resolution, it allows for the visual distinction of NO₂ plumes of individual ships. To successfully deploy a compliance monitoring system that is based on TROPOMI data, an automated procedure for the attribution of NO₂ to individual ships has to be developed. However, due to the extremely low signal-to-noise ratio, interference with the signal from other – often stronger – sources, and the absence of ground truth, the task is very challenging.

In this study, we present an automated method for segmentation of plumes produced by individual ships using TROPOMI satellite data – a first step towards the automated procedure for global ship compliance monitoring. We develop a multivariate plume segmentation method based on various ships', wind's and spatial properties. For this, we propose to automatically define a region of interest – a ship sector that we normalize with respect to scale and orientation. We create a dataset, where each pixel has a label for belonging to the respective ship plume or not. We train five linear and nonlinear classifiers. The results show a significant improvement over the threshold-based baselines. Moreover, the aggregated NO₂ levels of the segmented plumes show high correlation with the theoretically derived measure of ship's emission potential.

KEYWORDS

TROPOMI, NO₂, shipping, Moran's I, AIS, wind, IMO, multivariate model, supervised classification, ship plume segmentation

1 INTRODUCTION

As of 2021, the International Maritime Organization has significantly tightened the regulations regarding the NO_x emission for ships operating in the Baltic and North Sea waters [19]. This decision was justified by the fact that the international shipping sector is one of the strongest sources of anthropogenic emission of NO_x –

a substance harmful both for human health and ecology. The contribution of the shipping industry is estimated to vary from 15% to 35% worldwide [12], [20], which leads to approximately 60,000 premature deaths annually [11]. And, while over the last 20 years the pollution produced by power plants, the industry sector and cars has been constantly decreasing, the impact of the maritime transport continues to grow fast [8].

All methods currently used for ship compliance monitoring such as in-situ [3], [25], on-board [1], and airborne platform-based [37] have several disadvantages: they all require close proximity to a ship, they are costly, and they do not allow ship compliance monitoring on a global scale. A potential solution to the problem is the application of remote sensing instruments [31], such as the TROPOMI/S5P satellite [38] that was launched in 2018. Studies [15], [21] show that traces of NO₂ plumes produced by individual ships can be manually distinguished on TROPOMI images.

The first step required for the development of a scalable automated remote sensing-based compliance monitoring system is an automated method for the evaluation of NO_x emission produced by individual ships. In order for such an evaluation to be successful, the following challenges have to be addressed:

- Denoising of satellite measurements.
- Ship-plume segmentation.
- Assignment of the detected plume to a ship.

Image denoising. In the domain of image processing, the classical approach for image smoothing and noise removal is the application of convolution-based filters [10]. The convolutional operator locates the filter matrix centered on the original image pixel and returns the output as the sum of the element-wise product of the filter matrix and the patch of an analyzed image covered by the filter [17]. However, in the case of the TROPOMI satellite, the dimensions of a patch of a ship plume will not be larger than 18 × 18 pixels. Consequently, the application of a convolution-based filter will lead to a significant information distortion. For instance, two separate ship plumes blurred by a convolution filter may not be separable anymore.

Another challenge we have to deal with when using TROPOMI data for an estimation of the amount of NO₂ produced by individual ships is the lack of the repeatability of the signal. Due to the extremely low sample rate (1 sample per day) of satellite images

as well as high complexity of the factors (such as atmospheric conditions, wind, neighborhood of the analyzed ship) that affect the shape and intensity of the detected plume we cannot treat two subsequent images of plumes produced by the same ship as two images of the same plume. For this reason, none of multiple images-based methods of an image reconstruction or foreground detection (e.g. [28], [30]) can be applied to our problem.

Plume segmentation. Task of ship plume segmentation can be compared with the non-trivial problem of sky clouds segmentation. The main difficulties of both tasks are a non-rigid structure of an analyzed object, and absence of clear borders or other discriminative features that can be extracted by supervised learning models. Trying to overcome this, the majority of cloud segmentation models [23], [22], [13] are focused on the maximally efficient usage of the only relevant discriminating feature: color. However, all above mentioned studies work with 3-channels RGB images. When dealing with a single-channel TROPOMI NO₂ data, the information content is limited even more.

The current state-of-the-art approach for segmentation of images of a small size is a widely used for biological applications (e.g. [6], [9]) U-Net architecture. In case of medical imaging, however, the size of images rarely goes below 128x128 pixels. With the image size available to us, an essential for the U-Net sequence of pooling-based image size reductions becomes infeasible.

Ship-plume assignment. When the NO₂ plumes are separated from the background, the next step is to assign the segmented plume to a corresponding ship. For this purpose, the known information about ships' trajectories has to be associated with the TROPOMI pixels. For several reasons this is a difficult problem. First, a plume produced by a ship will be shifted and displaced by the wind. As a consequence, any uncertainties in wind information ([7], [35]) will lead to possible misassignments. Second, not all plumes that are visually distinguishable on TROPOMI images can be associated with a ship. For instance, while all bigger commercial vessels are obliged to report their positions, military ships can travel incognito, producing NO₂ plumes that cannot be associated with any ship available in data records. Other possible open sea sources of unmatchable NO₂ plumes are gas drilling stations, or remainings of pollution plumes originating from land. Finally, a close proximity or intersection of plumes of several ships make the task even more complex.

Our contribution. Here, we present a novel methodology for segmentation of NO₂ plumes from individual ships using multivariate supervised learning models on TROPOMI satellite data. First, we enhance an image using its properties of spatial auto-correlation. This way, we reduce the magnitude of noise without blurring the image. Then, for each analyzed ship, we perform an automatic generation of a Region of Interest (ROI) - a ship sector, which later is normalized and divided into sub-regions. With this, we introduce a new method of feature construction that enables us to approach the problem of ship plume segmentation with multivariate models. As a next step, we utilize newly generated features to create a dataset that combines information from multiple data sources. We manually label the data as a "plume" and "not plume" pixel, which allows us to solve the problem of segmentation of plumes from individual ships using supervised learning. Finally, we compare the performance of five linear and nonlinear multivariate supervised

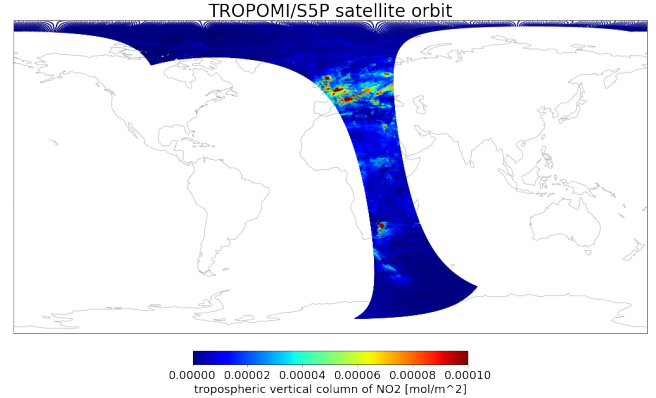


Figure 1: Illustration of a TROPOMI/S5P satellite orbit. In 24 hours the satellite covers the full globe.

classification models, and validate the estimated based on the segmentation results, amount of NO₂ from an individual ship, with the theoretically derived measure of ship emission potential. To sum up, our contribution can be listed as follows:

- Development of a novel multi-subregion based method of feature construction that allows to address the problem of ship-plume segmentation in a multivariate manner.
- Preparation and labeling of a new, composed of several data sources dataset, which for the first time allows a supervised learning on TROPOMI data.
- Comparison of the obtained results with the theoretically derived measure of ship emission potential.

The rest of this paper is organized as follows: in Section 2, we start with the description of data sources used in this study. We then present an overview of the relevant literature in Section 3. In Sections 4 and 5, the reader can find the descriptions of the proposed method and the experiment design, respectively. Finally, in Section 6, we present the results of the study, followed by the conclusions in Section 7.

2 DATA SOURCES

In this paper, we perform an integration of three data sources: TROPOMI satellite measurements, wind data, and information about the ships' positions. In this Section, the used data is described in detail.

2.1 TROPOMI data

TROPOMI/S5P [38] is a spectrometer on board of the Copernicus Sentinel 5 Precursor satellite. The satellite was launched in October 2017 and entered its operational phase starting from May 2018. The TROPOMI/S5P data is freely available via <https://s5phub.copernicus.eu/>. The spectrometer measures several trace gases including NO₂. Since the NO₂ gas is the most notable product of photochemical reactions of NO_x emitted by ships, it can be utilized for the monitoring of the ships' emission compliance. In 24 hours the satellite performs approximately 14 orbits and with these covers the full globe. Figure 1 provides an example of a satellite orbit. Excluding some rare exceptions, each point of the globe will be captured by the

satellite only once in 24 hours. The maximal ground pixel resolution for the instrument is equal to $5.5 \times 3.5 \text{ km}^2$. Due to the projection of the satellite images, the real size of the pixel will vary, depending on the true distance between the satellite and the part of the surface of the earth being imaged. To generate images of a regular size, we regridded¹ the original TROPOMI data into regular-size grid of a size of $0.045^\circ \times 0.045^\circ$, which translates to approximately $5 \times 5 \text{ km}^2$. To assure the high quality of the analyzed pixels, some filtering criteria were applied on the satellite data (for details, see Appendix C).

The wind information was obtained from wind speed data from the European Center for Medium range Weather Forecast at 10 m height, available with 0.25° resolution at 6-hourly time steps².

2.2 Ship-related data

Another source of data used in this study is data from AIS transponders³. The data include position, speed, heading and a unique identifier (MMSI) of each ship carrying an active transponder. Due to the fact that at the moment there are no open access AIS data available, the data were provided to us by the Human Environment and Transport Inspectorate (ILT) of the Netherlands. Information about dimensions of the ships we retrieved from official ship registries.

3 RELATED WORK

Since the TROPOMI/S5P mission is still relatively new, only limited amount of studies bears relevance to this work. It was reported that the NO_2 plumes produced by individual ships can be visually distinguished on TROPOMI data [15]. The authors introduced the method of wind shifted track of a ship, which has become a basis for a ship-plume assignment procedure. However, an emission plume quantification technique presented in the study was entirely manual.

Next, we introduced the first attempt of an automated evaluation of NO_2 produced by individual ships [21] and discussed the importance of TROPOMI data enhancement for the problem of plume-background separation. The plume-background separation itself, however, was based on an unsupervised method of a threshold, established individually for each of analyzed ships. This approach lacks flexibility, resulting in assignment of noisy pixels to a ship. Moreover, because of the absence of ground truth, there was no possibility to fully optimize the threshold. Finally, with the one-feature based method of thresholding the spatial information is completely ignored, what, among others, does not allow to differentiate the plume produced by the analyzed ship from all the other NO_2 plumes that might be located in the ship's proximity.

The earlier set of works was focused on the quantification of the emission from shipping with the predecessors of TROPOMI/S5P. Using the measurements from the GOME instrument, the NO_2 emission level above the shipping lane between Sri Lanka and Indonesia was estimated [5]. With the SCIAMACHY satellite images, traces from shipping industry over the Red Sea were quantified

[29]. Finally, OMI satellite data was used to visualize a ship NO_x emission inventory for the Baltic Sea [39]. Nevertheless, due to the low resolution capabilities of above-mentioned predecessors of TROPOMI/S5P (GOME: $40 \times 320 \text{ km}^2$, SCIAMACHY: $30 \times 60 \text{ km}^2$, OMI: $13 \times 25 \text{ km}^2$), these studies were based on multi-month data averaging, which does not give the possibility to quantify emission from individual ships.

Lastly, there are several studies demonstrating the capability of TROPOMI NO_2 measurements to pinpoint the emission from urban (e.g. [4], [24]) or industrial sources, such as mining industry [18], or a gas pipeline [36], as well as showing the possibility of the usage of TROPOMI data to quantify the positive effects of COVID-19 lockdown (e.g. [14]). Nonetheless, since all studied emission sources are stationary (thus can be observed over an extended period of time) and emitting much higher quantities of NO_x than an individual ship, all the above-mentioned problems are arguably less complex than the one discussed in this paper.

4 METHOD

In this Section, we present our method that allows to translate the spatial information contained in TROPOMI images into a set of features, enabling the application of multivariate supervised models for the task of ship-plume segmentation. The method consists of the following steps: an AIS data-based interpolation of the ship tracks at the moment and just before the satellite overpass, definition and enhancement of a ship plume image, definition of a ship sector that allows the further restriction of the analyzed area, normalization of the defined ship sector and further it split into smaller sub-regions, which, finally, gives the possibility to retrieve the set of necessary features. These steps are described below.

4.1 Ship tracks

First step is to estimate the tracks of the studied ships from two hours before to the moment of satellite overpass. This period is chosen such that the pixels representing the trace of the ship closely match the plume size in length, which can vary for several reasons (for example, due to the seasonal influence on signal-to-noise ratio, half-life of NO_2 in the atmosphere, or weather related influence on the dispersion time).

We distinguish two types of ships'-tracks: the *ship track*, obtained based on resampling and interpolation of the AIS data, and the *wind-shifted ship track*, calculated by moving the coordinates of the *ship track* in accordance with the speed and direction of the local wind. The *ship track* provides us the information on the position of the ship, where the studied ship plume was emitted from. The *wind-shifted ship track* indicates the expected position of the NO_2 plume that was produced by the ship, and moved over time by the prevailing wind. Figures 2(c) and 2(d) give examples of the *ship track* and its corresponding *wind-shifted ship track* respectively.

4.2 Ship plume image

Utilizing the knowledge of a ship's position summarized in its *ship track* and *wind-shifted ship track*, we are able to focus our attention to the area that lies within an immediate proximity to the analyzed ship. For this, the concept of a *ship plume image* (see Figure 2(a)) is introduced. The area of the *ship plume image*

¹For the data regridding HARP v.1.13 Python package was utilized.

²Starting from product version upgrade from 1.2.2 to 1.3.0 that took place on March 27, 2019, the ECMWF wind data is available as a support product in the TROPOMI/S5P data file.

³Since 2002 all commercial sea-going vessels are obliged to carry on board an AIS transponder [26].

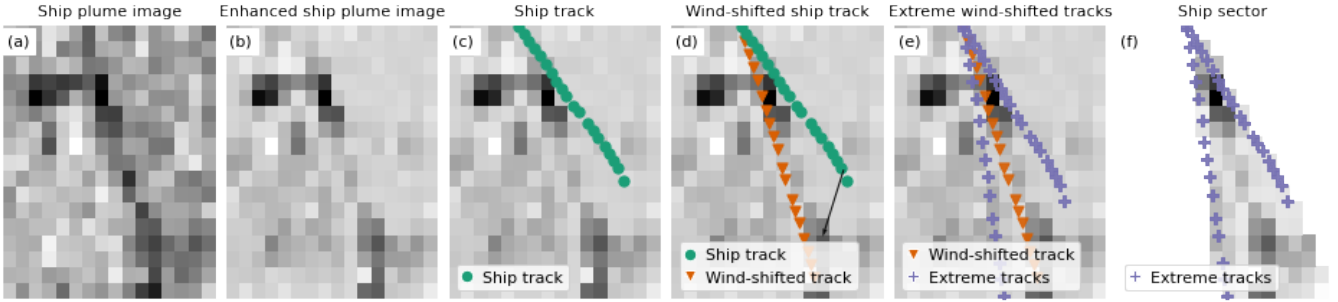


Figure 2: Ship sector definition pipeline. (a) *Ship plume image* - the TROPOMI NO₂ signal for the area around the analyzed ship. Three ship plumes can be distinguished, but only one is of interest. (b) The NO₂ signal enhanced by Moran's I spatial auto-correlation statistic. (c) *Ship track* - estimated, based on AIS data records. (d) *Wind-shifted ship track* - a ship track shifted in accordance with the speed and direction of the wind. The *wind-shifted ship track* indicates an expected position of the ship plume. A black arrow indicates the wind direction. (e) *Extreme wind-shifted ship tracks* - calculated, based on wind information with assumed uncertainties; define the borders of the *ship sector*. (f) The resulting *ship sector* - the ROI of an analyzed ship.

is determined based on a *wind-shifted ship track* as follows: the average coordinate of the studied *wind-shifted ship track* defines the center ($longitude_{centr}, latitude_{centr}$) of the *ship plume image*, the borders of the image are defined as $longitude_{centr}, latitude_{centr} \pm 0.4^\circ$. This particular size of a *ship plume image* was determined as optimal for ship plume coverage, based on results of manual inspection of a set of ship plume images, given the speed of the ship and the wind. Given the size of the pixel grid, such an offset results in an image of a maximal dimension of 18×18 pixels.

4.3 Enhancement of a ship plume image

When the images are defined, the next step is to enhance the contrast between the ship plume and the background. Since the information content of the image is very limited, we chose to utilize spatial auto-correlation, that enables us to quantify how the value of a certain pixel is related to the values of pixels in its neighborhood [33]. Thus, calculating the spatial auto-correlation of a *ship plume image*, we pinpoint the only feature that differentiates the ship plume - a cluster of high value pixels adjacent to each other, from the background - a mixture of pixels of different, often comparable intensity.

For the quantification of the spatial auto-correlation of a *ship plume image*, we use the spatial auto-correlation statistic local Moran's I [2] - the most popular measure of spatial auto-correlation in image processing [34]. For a pixel i , the local Moran's I is defined as:

$$I_i = \frac{(x_i - \mu)}{\sigma^2} \sum_{j=1, j \neq i}^N w_{ij}(x_j - \mu), \quad (1)$$

where x_i is the value of the respective pixel, N is the number of analyzed pixels of an image (in our case 18×18), μ is a mean value of all N pixels, σ^2 their variance, and w_{ij} is the value of an element in a binary spatial contiguity weight matrix W at location j with regards to the analyzed pixel i . The value of an element of the binary spatial contiguity matrix w_{ij} is 1 for pixels that are considered to be the neighbors of the analyzed pixel i , and 0 otherwise. In this study, we use the queen spatial contiguity [16], which is the 3×3 8-neighborhood of the analyzed (central) pixel.

In case of an NO₂ ship plume - a group of pixels with a value higher than μ located next to each other, it will lead to a high Moran's I value for each of those pixels. On the other hand, if a high value pixel is surrounded by pixels of a non-uniform concentration, it will be treated as noise and the corresponding Moran's I value will be lower. An example of a result of an *enhanced ship plume image* is provided in Figure 2(b).

A disadvantage of the usage of the spatial auto-correlation is the fact that the clusters of low values will be enhanced along with the clusters of high NO₂ value. In case of a rare event of images with a clean uniform background, such behavior of the statistic can be misleading.

4.4 Ship sector

A plume produced by a ship at a given moment will be displaced, over time, in the direction of the prevailing wind. Therefore, having the wind information available, we can narrow the analysis to the part of the *ship plume image*, where the probability to find the plume of the ship is the highest. To achieve this, for each analyzed ship, we define a Region of Interest (ROI), or *ship sector*. As a starting point of the *ship sector*'s definition, we use the calculated based on available wind information, *wind-shifted ship track*. We then, calculate the *extreme wind-shifted tracks* by adding the margin of wind-related uncertainty to either side of the *wind-shifted ship track*. The *extreme wind-shifted tracks* delineate the borders of the *ship sector*, showing the extreme possible positions of the plume, taking the wind measurement uncertainty into account. The wind uncertainty is assumed due to the limited spatial and temporal resolution of wind data [15] and, reported in several studies ([7], [35]) measurement bias. Illustrations of the *extreme wind-shifted tracks* and the resulting *ship sector* are shown in Figures 2(e) and 2(f), respectively. Based on our assumptions, the plume always lies within the *ship sector* boundaries; thus, only pixels lying within the *ship sector* are taken into consideration in further analysis. All parameters related to the *ship sector* can be found in Appendix A.

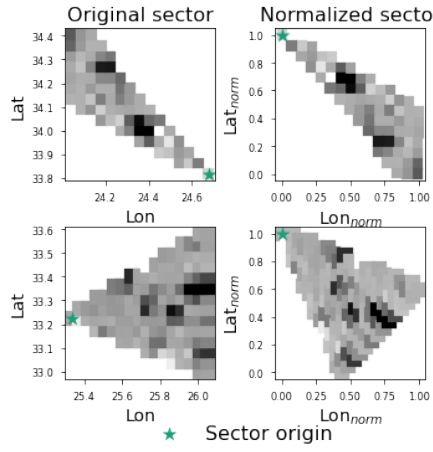


Figure 3: Sector normalization. We rotate the *ship sectors* so that all resulting sectors have the same orientation independently on the original direction of the ship's heading. We then rescale the image so that the range of both coordinates is between 0 and 1. The sector origin indicator shows the position of the ship at the moment that the image was taken.

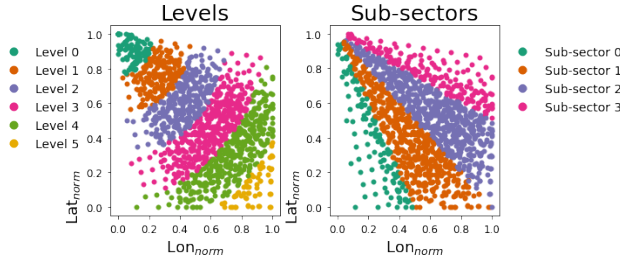


Figure 4: Levels and sub-sectors. We perform a feature construction by dividing the *normalized sector* into sub-regions: *levels* and *sub-sectors*.

4.5 Feature set construction

In order to obtain a multivariate description of the *ship sector* pixels, we encode the spatial information into a set of features. First, we perform a *ship sector* normalization. We define a *normalized sector* by standardization of the orientation and the scale of the *ship sector* (see Figure 3). In this way, the position of the plume within the *ship sector* becomes invariant to the heading (direction) and speed of the ship, as well as to the direction and speed of the wind. We standardize the orientation of a *ship sector* by rotating to 320° , such that the angle of the polar coordinate of the corresponding *wind-shifted ship track* is the same for all ships. This particular value of sector rotation angle was chosen for convenience of visualization and has no influence on the further modelling. We standardize the *ship sector*'s scale so that the horizontal and vertical coordinates of the rotated *ship sector* are rescaled into the range $[0, 1]$.

The second step of the feature construction procedure is the division of the *normalized sector* into a set of sub-regions that enable to encode spatial information of the pixels within the *normalized*

sector. We perform a radial and angular division of the *normalized sector* creating *sub-sectors* and *levels* respectively. For illustration, see Figure 4. As a result of this division, the position of each pixel within the *normalized sector* image can be characterized in terms of two values: a *level* and *sub-sector*.

5 EXPERIMENT DESIGN

Here, we describe the experimental set up used in this study: first, we describe the dataset used for the training of the multivariate models, then we explain the models used for the benchmarking, as well as provide list the used multivariate classifiers. In addition, in this section, the reader can find the description of the methods used for the models' optimization and measures utilized for the models' performance evaluation.

5.1 Dataset composition

The dataset was composed out of 68 days of NO_2 TROPOMI satellite measurements collected during the period between 1 April, 2019 and 31 December, 2019. For the analysis, an area in the Mediterranean Sea, restricted by the following coordinate range: lon: $[14^\circ; 31.5^\circ]$, lat: $[30^\circ, 38^\circ]$ was chosen. This particular region was selected because of the high amount of sunny days, and comparably low levels of NO_2 pollution, which are favourable conditions for the analysis. An outline of the area studied can be found in Figure 8 of Appendix C.

Because of the complexity of this analytical task, we focus on ships that are spatially separable, and producing substantial amounts of NO_2 . Since the size of an NO_2 plume grows with the speed of the ship, which is directly related to the probability of detection from the satellite data, only ships with a speed that exceeds 14 kt⁴ were taken into consideration. Furthermore, if two ships move in close proximity to each other, creating duplicate images, only the image related to the ship with the highest speed was taken into consideration. In this way, 754 images were created and limited to an area of *ship sector*. The enhanced by Moran's *I* *ship sector* images were then manually labelled. To support the labeling process, the raw (NO_2) *ship sector* images and the full Mediterranean Sea area images were available to the labeler as reference information. The full list of analyzed dates along with the number of resulting images per day can be found in Figure 9 of Appendix C. The resulting dataset is composed of 6980 pixels labeled as "plume" and 68646 pixels labeled as "not plume". The dataset is unbalanced. More descriptive statistics of the dataset are provided in Appendix C.

5.2 Benchmarks

In this subsection, we describe the used benchmark methods. To validate the proposed approach of feature construction, all benchmarking models are based on an optimization of a threshold applied to a single feature being a row value of NO_2 from within the *ship sector*, Moran's *I* enhanced value of the *ship sector* image pixels, or the value of Moran's *I* statistic applied exclusively on the high value *ship sector*'s pixels. All used thresholds were optimized using manually labeled data, so that the quality of ship-plume separation is maximized.

⁴kt - knot, a unit of speed equal to a nautical mile per hour. 14 kt \approx 7.2 m/s.

The first benchmark method was based on thresholding of Moran's *I* enhanced *ship sector* images. The main limitation of this method is the fact that the clusters of low concentration will also be separated, even though they are not the part of a plume. Therefore, the precision of such a model potentially will be lower. To overcome this problem, we propose to assign the zero value to all pixels of the image with intensity lower than the median of the given *ship sector* picture, and afterwards apply the Moran's *I* enhancement. This is a second method used for the benchmarking, which we call *Moran's I on high NO₂*. The last benchmark model uses a threshold on the raw NO₂ values. The main risk associated with this method is the high sensitivity to the noise presence in the data. The common disadvantage of all above mentioned models is the fact that none of these thresholding-based methods can make use of the spatial information within the ship sector.

5.3 Multivariate models

To exploit the potential of multivariate modelling we used several classifiers of increasing complexity: Logistic Regression, Support Vector Machines with linear kernel, Support Vector Machines with radial basis kernel (RBF SVM), Random Forest⁵, and Extreme Gradient Boosting (XGBoost)⁶. The above mentioned models were able to benefit from ship and wind related features, along with the set of spatial features developed with the method described in Subsection 4.5.

The first feature used is the Moran's *I* enhanced values of the pixels that were translated into a feature vector. Apart from the values of Moran's *I*, the feature set was composed of the corresponding value of NO₂, Wind Speed, Wind Direction⁷, Ship Speed, and Ship Length. Finally, the position of an analyzed pixel within the *normalized sector* in terms of *levels* and *sub-sectors* was translated into the feature vectors using one-hot encoding. The resulting feature set was composed of 17 features in total. The used binary label indicates whether the given pixel is part of the ship plume or not.

5.4 Segmentation validation metrics

For the assessment of classification quality, we used the list of evaluation metrics being: Precision - a measure of how many of samples that were predicted as positive are actually positive. Recall - a measure of how many of the actual positive samples have been identified by the model as positive. The F1 score - harmonic mean of the precision and recall. The average precision score (AP)⁸ - is given by the area under the precision-recall curve.

5.5 Cross-validation and parameters optimization

For the model fine-tuning and model performance evaluation, nested cross-validation was used. In the inner loop, we performed a randomized grid-search with 5-fold cross validation to optimize all hyperparameters of the methods compared in the experiments. The

⁵All above-mentioned models were implemented in Scikit-learn v. 0.24.2 package[27]

⁶Implemented in xgboost Python package v. 1.3.3.

⁷Wind Direction feature vector was encoded into its sine and cosine components, in order to enable a continuous feature space for various wind directions.

⁸All above-mentioned evaluation metrics were implemented in Scikit-learn v. 0.24.2 package[27].

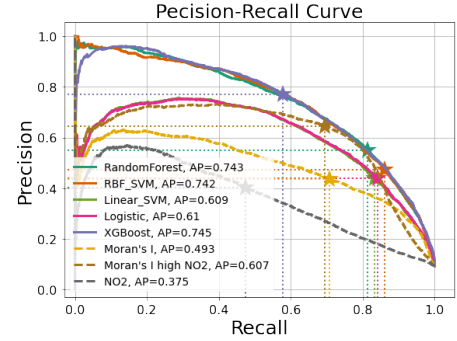


Figure 5: Precision-recall curve based on 5-fold cross-validation. Dashed lines indicate models used for the benchmarking. Stars indicate thresholds as optimized by the respective models.

AP score was used as a target function for the optimization of the multivariate models, while F1-score, which optimizes the binary responses of the classifier, was used for the optimization of the values of the thresholds used for the benchmark models. In the outer loop, the 5-fold cross validation served for the evaluation of the quality of the models' performance. To prevent the situation where the pixels originated from the same ship plume image ends up in two different sets (training-test set, training-validation set), a non-overlapping group dataset split strategy was used both for inner and outer loop cross validations. The search space of the hyperparameters for each of the analyzed multivariate models is provided in Appendix B. For Logistic Regression, Linear SVM, RBF SVM, and Random Forest the information of class imbalance was provided as calculated on the train set with a class weight matrix. The XGBoost classifier is able to directly optimize the responses using the Average Precision score as a target function.

5.6 NO₂ validation metrics

Using the pixel classification, it is possible to measure how well the separated plume represents the amount of NO_x that has been produced by an analyzed ship. For this purpose, we used a ship emission proxy [15] that is defined as:

$$E_s = L_s^2 \cdot U_s^3, \quad (2)$$

where L_s is the length of the ship in m , and U_s is its speed in m/s . The proxy does not give us an exact amount of the NO_x produced by the ship, but provides a relative score of the emission potential of the analyzed ships. We used the NO_x emission proxy to compare with the summarized for each ship levels of NO₂ - a chemical product of NO_x emitted by ships that can be measured with TROPOMI. Since the above measures cannot be compared directly, to validate the quality of NO₂ estimation, we used the Pearson correlation between the emission proxy and the estimated level of NO₂.

6 RESULTS

6.1 Plume segmentation

In Table 1 we report the results of the pixel classification based on 5-fold cross validation for all models and baselines studied. Figure

Model	Precision	Recall	F1	AP
Linear SVM	0.438±0.028	0.833±0.022	0.573±0.029	0.609± 0.063
Logistic	0.439±0.030	0.841±0.024	0.576±0.030	0.610±0.064
RBF SVM	0.474±0.030	0.861±0.020	0.611±0.029	0.742±0.031
Random Forest	0.548±0.020	0.813±0.017	0.654±0.019	0.743±0.030
XGBoost	0.770±0.027	0.577±0.035	0.659±0.030	0.745±0.030
Moran's <i>I</i>	0.435±0.043	0.707±0.029	0.538±0.039	0.493±0.063
Moran's <i>I</i> on high NO ₂	0.645±0.033	0.694 ±0.034	0.669±0.033	0.607±0.056
NO ₂	0.403±0.051	0.475 ±0.027	0.435±0.038	0.375±0.062

Table 1: Results on the test set with 5-fold cross-validation. Bold font indicates best results obtained for a given measure.

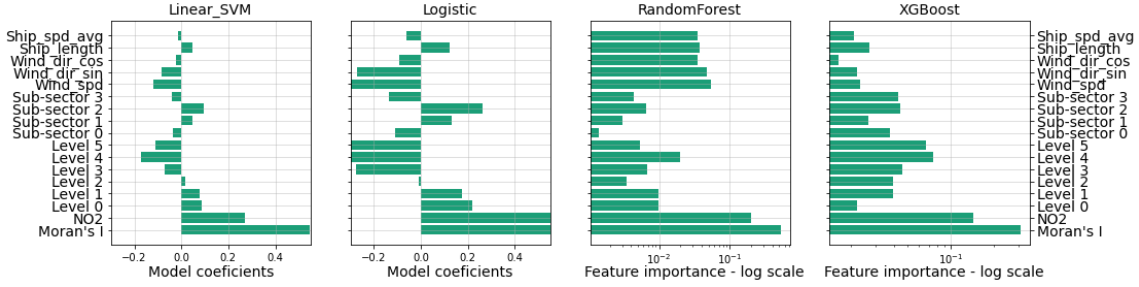


Figure 6: Coefficients of the features in the decision function of the linear models and the impurity-based feature importance values for tree-based models.

5 provides the corresponding precision-recall curves, obtained by aggregating the scores over all cross-validation "hold out" sets. In Figure 6 we visualize the model coefficients for the linear models studied, as well as the impurity-based feature importance coefficients for the tree based models (Random Forest and XGBoost). The obtained results can be summarized as follows: (i) All multivariate models utilize the spatial information provided by sub-sectors and levels. Even though, the coefficients' values depicted in Figure 6 cannot be compared directly, due to the different nature of the models, the relative differences between the models' features go along with our intuition on where the plume produced by an analyzed ship should be located within a *normalized sector*. For instance, high negative coefficients for the linear models that correspond to the features *Level 4* and *Level 5* suggest that even if a high value pixel does occur in those regions of *normalized sector*, it most probably was produced by a source other than analyzed ship. On the other hand, the high positive coefficients corresponding to a feature *Sub-sector 2*, tells us that if a high value pixel occurs in the middle of the sector, it is most probably a part of the plume produced by the studied ship. (ii) Nonlinear classifiers clearly outperform both linear classifiers and threshold based benchmarks, providing the possibility to achieve a very high level of precision given a reasonable level of recall. Moreover, a significantly lower level of standard deviation of AP scores suggests that results obtained with the nonlinear classifiers are more robust.

6.2 NO₂ validation results

In Figure 7, we provide the results of the comparison between NO₂ values estimated for a given ship on a given day by the classification

results and the theoretically derived emission proxy. The results show that the XGBoost classifier outperforms all studied models, while the performance quality of the other models cannot be clearly differentiated. The highest contrast between the scores of the performance metrics and the correlation with the emission proxy can be noted for the NO₂ thresholding benchmark model. This, however, results in the ship plumes composed out of one pixel that were not labeled as plumes. The substantially high correlation with the emission proxy, however, suggests that the single-pixel plumes were correctly identified by the method. From Figure 7 we can also see that the number of plumes identified by the studied models is often higher than the number of plumes labeled. These "false positives" might suggest that the best machine learning set-ups are able to do a better ship-plume segmentation than the human labeler. Illustrations of both above-mentioned examples can be found in Appendix D.

7 CONCLUSIONS

In this study, we presented a method for an automatic segmentation of NO₂ plumes produced by individual ships. We started with an automatic assignment of an ROI – a *ship sector* to each analyzed ship. We performed a *ship sector* normalization and then divided it into smaller *levels* and *sub-sectors*. This enabled us to construct a set of features, which in turn gave the possibility to transform the thresholding problem of a ship plume segmentation into a multivariate model. We created and manually labeled a dataset, where multiple data sources were combined. The labeled dataset allows to address the problem of individual ship-plume segmentation in a

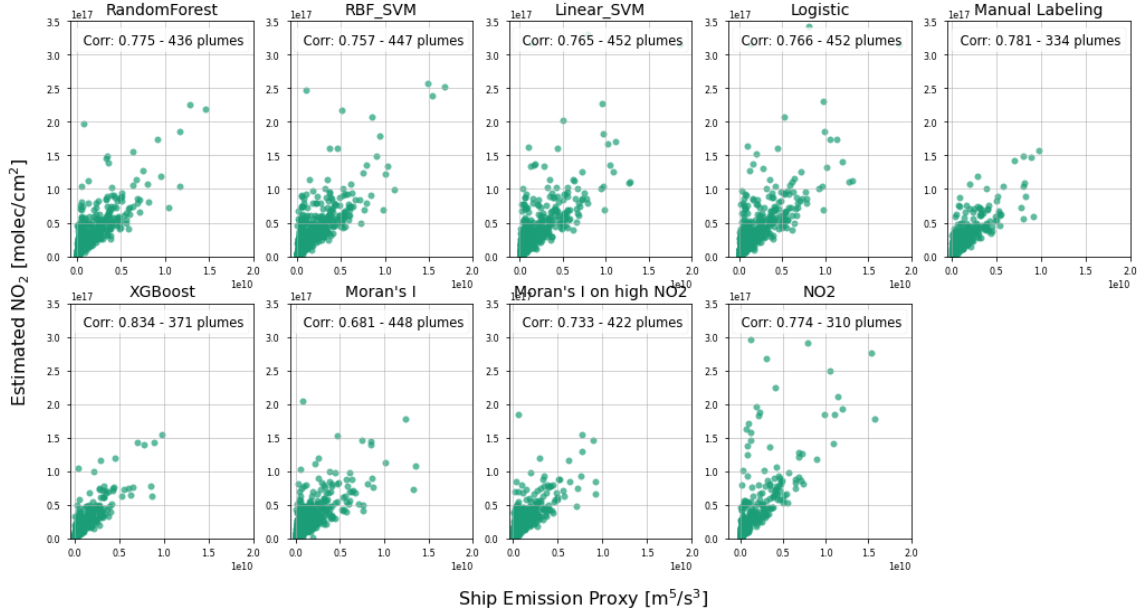


Figure 7: Pearson correlations between estimated (based on classification results) values of NO₂ emitted by each ship on a given day and a theoretically derived measure of ship emission potential – ship proxy.

supervised manner. We trained a set of linear and nonlinear classifiers and showed that nonlinear classifiers significantly outperform all the thresholding-based baselines and the linear models. Finally, we estimated the amount of NO₂ produced by each of the analyzed ships by segmentation results of our models, and compared it with a theoretically derived NO_x ship emission proxy. High correlations show that our methodology provides a way to rank the analyzed ships in terms produced NO_x. This means that the method is ready to become a basis for further development of a TROPOMI based ship compliance monitoring procedure. In addition, with the XG-Boost model, we were able to achieve a higher correlation between the estimated NO₂ and the emission proxy than with manual labeling, while also being able to detect more ship plumes. This fact leads to the conclusion that the model is able to correctly segment plumes that were not identified by the labeler. However, further investigation of this topic is required and will be a subject of future studies.

Summing up, the presented approach allows for the first time to use the TROPOMI/S5P satellite data for the supervised segmentation of NO₂ plumes produced by individual seagoing ships. This brings us a step closer to the development of a global and continuous system of ship compliance monitoring that will enable an effective enforcement of IMO regulations.

ACKNOWLEDGMENTS

This work is funded by the Netherlands Human Environment and Transport Inspectorate, the Dutch Ministry of Infrastructure and Water Management, and the SCIPPER project, which receives funding from the European Union's Horizon 2020 research and innovation programme under grant agreement Nr.814893.

REFERENCES

- [1] Harshit Agrawal, Quentin GJ Malloy, William A Welch, J Wayne Miller, and David R Cocker III. 2008. In-use gaseous and particulate matter emissions from a modern ocean going container vessel. *Atmospheric Environment* 42, 21 (2008), 5504–5510.
- [2] Luc Anselin. 1995. Local indicators of spatial association—LISA. *Geographical analysis* 27, 2 (1995), 93–115.
- [3] Jörg Beecken, Johan Mellqvist, Kent Salo, Johan Ekholm, and J-P Jalkanen. 2014. Airborne emission measurements of SO₂, NO_x and particles from individual ships using a sniffer technique. *Atmospheric Measurement Techniques* 7, 7 (2014), 1957–1968.
- [4] Steffen Beirle, Christian Borger, Steffen Dörner, Ang Li, Zhaokun Hu, Fei Liu, Yang Wang, and Thomas Wagner. 2019. Pinpointing nitrogen oxide emissions from space. *Science advances* 5, 11 (2019), eaax9800.
- [5] S Beirle, U Platt, R Von Glasow, M Wenig, and T Wagner. 2004. Estimate of nitrogen oxide emissions from shipping by satellite remote sensing. *Geophysical Research Letters* 31, 18 (2004).
- [6] Laurens Beljaards, Mohamed S Elmahdy, Fons Verbeek, and Marius Staring. 2020. A Cross-Stitch Architecture for Joint Registration and Segmentation in Adaptive Radiotherapy. In *Medical Imaging with Deep Learning*. PMLR, 62–74.
- [7] Maria Belmonte Rivas and Ad Stoffelen. 2019. Characterizing ERA-Interim and ERA5 surface wind biases using ASCAT. *Ocean Science* 15, 3 (2019), 831–852.
- [8] K Folkert Boersma, Geert CM Vinken, and Jean Tournadre. 2015. Ships going slow in reducing their NO_x emissions: changes in 2005–2012 ship exhaust inferred from satellite measurements over Europe. *Environmental Research Letters* 10, 7 (2015), 074007.
- [9] Sijing Cai, Yunxian Tian, Harvey Lui, Haishan Zeng, Yi Wu, and Guannan Chen. 2020. Dense UNet: a novel multiphoton in vivo cellular image segmentation model based on a convolutional neural network. *Quantitative imaging in medicine and surgery* 10, 6 (2020), 1275.
- [10] Gustavo Camps-Valls, Devis Tuia, Luis Gómez-Chova, Sandra Jiménez, and Jesús Malo. 2011. Remote sensing image processing. *Synthesis Lectures on Image, Video, and Multimedia Processing* 5, 1 (2011), 1–192.
- [11] James J Corbett, James J Winebrake, Erin H Green, Prasad Kasibhatla, Veronika Eyring, and Axel Lauer. 2007. Mortality from ship emissions: a global assessment. *Environmental science & technology* 41, 24 (2007), 8512–8518.
- [12] Monica Crippa, Diego Guizzardi, Marilena Muntean, Edwin Schaaf, Frank Dentener, John A Van Aardenne, Suvi Monni, Ulrike Doering, Jos GJ Olivier, Valerio Pagliari, et al. 2018. Gridded emissions of air pollutants for the period 1970–2012 within EDGAR v4. 3.2. *Earth Syst. Sci. Data* 10, 4 (2018), 1987–2013.
- [13] Soumyabrata Dev, Yee Hui Lee, and Stefan Winkler. 2014. Systematic study of color spaces and components for the segmentation of sky/cloud images. In *2014*

IEEE International Conference on Image Processing (ICIP). IEEE, 5102–5106.

[14] Jieying Ding, Ronald J van der A, HJ Eskes, Bas Mijling, Trissevgeni Stavrakou, JHGM Van Geffen, and JP Veefkind. 2020. NO_x emissions reduction and rebound in China due to the COVID-19 crisis. *Geophysical Research Letters* 47, 19 (2020), e2020GL089912.

[15] Aristeidis K Georgoulias, K Folkert Boersma, Jasper van Vliet, Xiumei Zhang, Prodromos Zanis, Jos de Laat, et al. 2020. Detection of NO₂ pollution plumes from individual ships with the TROPOMI/S5P satellite sensor. *Environmental Research Letters* 15, 12 (2020), 124037.

[16] Arthur Getis and Jared Aldstadt. 2004. Constructing the spatial weights matrix using a local statistic. *Geographical analysis* 36, 2 (2004), 90–104.

[17] MC González-Sanpedro, Thuy Le Toan, J Moreno, L Kergoat, and E Rubio. 2008. Seasonal variations of leaf area index of agricultural fields retrieved from Landsat data. *Remote Sensing of Environment* 112, 3 (2008), 810–824.

[18] Debora Griffin, Xiaoyi Zhao, Chris A McLinden, Folkert Boersma, Adam Bourassa, Enrico Dammers, Doug Degenstein, Henk Eskes, Lukas Fehr, Vitali Fioletov, et al. 2019. High-resolution mapping of nitrogen dioxide with TROPOMI: First results and validation over the Canadian oil sands. *Geophysical Research Letters* 46, 2 (2019), 1049–1060.

[19] IMO. 1997. *Amendments to the annex of the protocol of 1978 relating to the international convention for the prevention of pollution from ships*. [https://wwwcdn.imo.org/localresources/en/KnowledgeCentre/IndexofIMOResolutions/MEPCDocuments/MEPC.75\(40\).pdf](https://wwwcdn.imo.org/localresources/en/KnowledgeCentre/IndexofIMOResolutions/MEPCDocuments/MEPC.75(40).pdf)

[20] Lasse Johansson, Jukka-Pekka Jalkanen, and Jaakkko Kukkonen. 2017. Global assessment of shipping emissions in 2015 on a high spatial and temporal resolution. *Atmospheric Environment* 167 (2017), 403–415.

[21] Solomiia Kurchaba, Jasper van Vliet, Jacqueline J Meulman, Fons J Verbeek, and Cor J Veenman. 2021. Improving evaluation of NO₂ emission from ships using spatial association on TROPOMI satellite data. In *Proceedings of the 29th International Conference on Advances in Geographic Information Systems*. 454–457.

[22] Qingyong Li, Weitao Lu, and Jun Yang. 2011. A hybrid thresholding algorithm for cloud detection on ground-based color images. *Journal of atmospheric and oceanic technology* 28, 10 (2011), 1286–1296.

[23] Charles N Long, Jeff M Sabburg, Josep Calbó, and David Pagès. 2006. Retrieving cloud characteristics from ground-based daytime color all-sky images. *Journal of Atmospheric and Oceanic Technology* 23, 5 (2006), 633–652.

[24] A Lorente, KF Boersma, HJ Eskes, JP Veefkind, JHGM Van Geffen, MB De Zeeuw, HAC Denier van der Gon, Steffen Beirle, and MC Krol. 2019. Quantification of nitrogen oxides emissions from build-up of pollution over Paris with TROPOMI. *Scientific reports* 9, 1 (2019), 1–10.

[25] Robert McLaren, Patryk Wojtal, Jamie D Halla, Cris Mihele, and Jeffrey R Brook. 2012. A survey of NO₂: SO₂ emission ratios measured in marine vessel plumes in the Strait of Georgia. *Atmospheric environment* 46 (2012), 655–658.

[26] Jun Min Mou, Cees Van der Tak, and Han Ligteringen. 2010. Study on collision avoidance in busy waterways by using AIS data. *Ocean Engineering* 37, 5-6 (2010), 483–490.

[27] F. Pedregosa, G. Varoquaux, A. Gramfort, V. Michel, B. Thirion, O. Grisel, M. Blondel, P. Prettenhofer, R. Weiss, V. Dubourg, J. Vanderplas, A. Passos, D. Cournapeau, M. Brucher, M. Perrot, and E. Duchesnay. 2011. Scikit-learn: Machine Learning in Python. *Journal of Machine Learning Research* 12 (2011), 2825–2830.

[28] Daniël M Pelt, Kees Joost Batenburg, and James A Sethian. 2018. Improving tomographic reconstruction from limited data using mixed-scale dense convolutional neural networks. *Journal of Imaging* 4, 11 (2018), 128.

[29] Andreas Richter, Veronika Eyring, John P Burrows, Heinrich Bovensmann, Axel Lauer, Bernd Sierk, and Paul J Crutzen. 2004. Satellite measurements of NO₂ from international shipping emissions. *Geophysical Research Letters* 31, 23 (2004).

[30] Christof Ridder, Olaf Munkelt, and Harald Kirchner. 1995. Adaptive background estimation and foreground detection using kalman-filtering. In *Proceedings of International Conference on recent Advances in Mechatronics*. Citeseer, 193–199.

[31] SCIPPER. 2020. *Shipping Contributions to Inland Pollution Push for the Enforcement of Regulations*. <https://www.scipper-project.eu/>

[32] Maarten Sneep. 2021. *Sentinel 5 precursor/TROPOMI KNMI and SRON level 2 Input Output Data Definition*. Technical Report S5P-KNMI-L2-0009-SD.

[33] Robert R Sokal and Neal L Oden. 1978. Spatial autocorrelation in biology: 2. Some biological implications and four applications of evolutionary and ecological interest. *Biological Journal of the Linnean Society* 10, 2 (1978), 229–249.

[34] Emma S Thompson, Pieter Saveyn, Marc Declercq, Joris Meert, Vincenzo Guida, Charles D Eads, Eric SJ Robles, and Melanie M Britton. 2018. Characterisation of heterogeneity and spatial autocorrelation in phase separating mixtures using Moran's I. *Journal of colloid and interface science* 513 (2018), 180–187.

[35] Ana Trindade, Marcos Portabella, Ad Stoffelen, Wenming Lin, and Anton Verhoef. 2019. ERAstar: a high-resolution ocean forcing product. *IEEE Transactions on Geoscience and Remote Sensing* 58, 2 (2019), 1337–1347.

[36] RJ van der A, ATJ de Laat, J Ding, and HJ Eskes. 2020. Connecting the dots: NO_x emissions along a West Siberian natural gas pipeline. *npj Climate and Atmospheric Science* 3, 1 (2020), 1–7.

[37] W Van Roy and K Scheldeman. 2016. Results MARPOL Annex VI Monitoring Report: Belgian Sniffer Campaign 2016. (2016).

[38] JP Veefkind, I Aben, K McMullan, H Förster, J De Vries, G Otter, J Claas, HJ Eskes, JF De Haan, Q Kleipool, et al. 2012. TROPOMI on the ESA Sentinel-5 Precursor: A GMES mission for global observations of the atmospheric composition for climate, air quality and ozone layer applications. *Remote sensing of environment* 120 (2012), 70–83.

[39] GCM Vinken, KF Boersma, A van Donkelaar, and L Zhang. 2014. Constraints on ship NO_x emissions in Europe using GEOS-Chem and OMI satellite NO₂ observations. *Atmospheric Chemistry and Physics* 14, 3 (2014), 1353–1369.

A SHIP SECTOR PARAMETERS

In Table 2, parameters used for the definition of ship sectors are provided.

Parameter	Value
Trace track duration	2 hours
Wind speed uncertainty	5 m/s
Wind direction uncertainty	40°

Table 2: Parameters applied for ship sector definition

B HYPERPARAMETERS SETTINGS

Below the reader can find the hyperparameters' search space that was used for the optimization of the multivariate model's performance, along with the hyperparameters that were always used for the model training.

- Linear SVM(*random_state*=0)
 - *C*: (2.0e-2, 2.0e-1, 2.0, 2.0e1, 2.0e2)
- Logistic(*solver*='saga', *l1_ratio*=0.5, *random_state*=0)
 - *penalty*: ('l1', 'l2', 'elasticnet', 'none')
 - *C*: (0.0001, 0.001, 0.1, 1)
 - *max_iter*: (100, 120, 150)
- RBF SVM(*kernel*='rbf', *gamma* = 'scale', *random_state*=0)
 - *C*: (2.0e-2, 0.5e-1, 1.0e-1, 1.5e-1, 2.0e-1, 2.5e-1, 2.0)
- Random Forest(*n_estimators*=500, *oob_score*=True, *random_state*=0)
 - *min_samples_leaf*: [2; 36]
 - *max_features*: ('sqrt', 0.4, 0.5)
 - *criterion*: ('gini', 'entropy')
- XGBoost(*objective*='binary:logistic', *eval_metric*='aucpr', *n_estimators*=500, *booster*='gbtree', *random_state*=0)
 - *gamma*: [0.05; 0.5]
 - *max_depth*: (2, 3, 5, 6)
 - *min_child_weight*: (2, 4, 6, 8, 10, 12)
 - *subsample*: [0.6; 1.0]
 - *colsample_bytree*: [0.6; 1.0]
 - *colsample_bylevel*: [0.6; 1.0]
 - *learning_rate*: (0.001, 0.01, 0.1, 0.2, 0.3, 0.4)
 - *reg_alpha*: (0, 1.0e-5, 5.0e-4, 1.0e-3, 1.0e-2, 0.1, 1)

C DATA DETAILS

In Table 3, the values that were applied on particular variables used for the quality filtering of TROPOMI data can be found. For detailed description of the variables see [32]. The data filtering is necessary to assure the highest possible quality of the TROPOMI signal. In Figure 8 we provide an example of the area used in this study. In Figure 9 the information about the dates used for this study as well

Parameter	Value
<i>qa_value</i>	>0.5
<i>cloud fraction</i>	<0.5

Table 3: TROPOMI data quality filters.

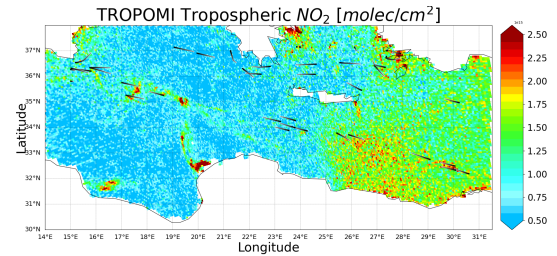


Figure 8: The NO₂ tropospheric column. An example of an analyzed area. Black lines indicate ships' tracks based on information from AIS data.

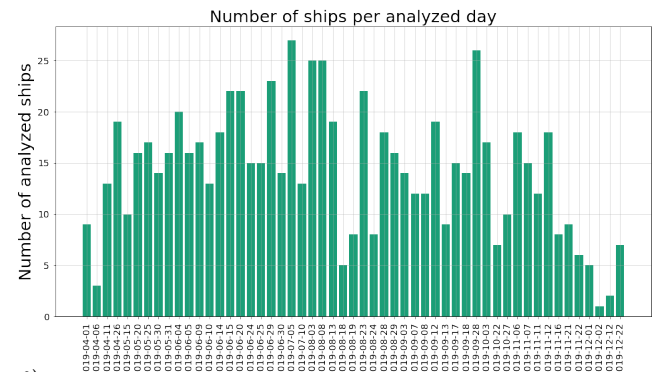


Figure 9: A list of days used for the dataset creation and an amount of ships per day studied.

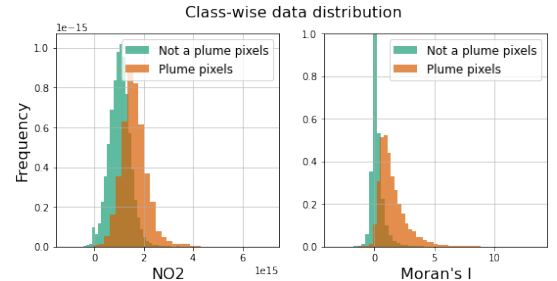


Figure 10: Class-wise distribution of the two main features of the dataset: NO₂ and Moran's I.

as number of ships per day studied is depicted. The differences in the numbers of ships per studied day can be caused by the lower traffic (for instance, during the vacation period), or, resulted in data losses, bad weather conditions of the measurement day.

In Figure 10 and Table 4 the information on the data distribution within the two classes of the dataset is shown. The mentioned numbers correspond to the full dataset before the training/test set division.



Figure 13: NO₂ based thresholding allows to distinguish plumes cumulated within the one pixel of TROPOMI image. Black pixels on the right hand side images indicate pixels, identified as a plume. Absence of black pixels means that there were no pixels within the area labeled as a plume.

	No plume	Plume
Number of pixels	68646	6980
Number of images	208	535

Table 4: Number of measurement points per class in the dataset.



Figure 11: XGBoost classifier allows to segment plumes that were not recognized by labeler. Black pixels on the right hand side images indicate pixels, identified as a plume. Absence of black pixels means that there were no pixels within the area labeled as a plume.



Figure 12: XGBoost - an example of misclassification. Black pixels on the right hand side images indicate pixels, identified as a plume. Absence of black pixels means that there were no pixels within the area labeled as a plume.

D DETAILS OF CLASSIFICATION RESULTS

In this section, we provide examples of the particular cases of ship plume segmentation. First, Figure 11 illustrates an example of a plume that has not been identified by the labeler as such, but was still classified correctly by the XGBoost classifier. High correlation with emission proxy (see Figure 7) suggests that segmentation was performed correctly. Figure 12 shows an example of the case, where the pixels of high NO₂ intensity have not been labeled as a plume, due to the fact that the origin of those pixels is different than the analyzed ship. The XGBoost classifier was not able to identify this correctly. In Figure 13 we give an example, when the plume produced by a ship is cumulated within a single TROPOMI pixel. It was not labeled as a plume by the labeler, and, because of the low value of Moran's *I*, has low chances to be classified as a plume by any of the supervised classifiers. Nevertheless, it was correctly segmented with the NO₂ threshold method.